AN IMPROVED YOLOV11N-BASED GENET FOR MISSING-SEED DETECTION AND COUNTING IN AN OBLIQUE HOOK-SHAPED SPOON-TYPE SMALL PRECISION SEED METERING DEVICE

/

基于改进 YOLOv11n 的斜勾勺式小型精量排种器漏播检测与计数模型 GENet

Wen SHIWEI [1], Zhang DEYI [1], Wei NAISHUO [1], Ge YAHAO [1], Chen JUN *[1], Huang TENGLONG *[1], Chen YU [1], Zhang SHUO [1], Bo HONGMING [2], Yuan WEI [3], Zhang BIN [4]

[1] College of Mechanical and Electronic Engineering, Northwest A&F University, Yangling 712100 / China
[2] Shangluo Agricultural Ecological Resources Protection Center, Shangluo 726000 / China
[3] Shangluo Agricultural Machinery Administration, Shangluo 726000 / China
[4] Shangluo Tengfei Agricultural Equipment Co., Ltd., Shangluo 726000 / China
Tel: +86-13572191773; E-mail: chenjun_jdxy@nwsuaf.edu.cn; htenglong@126.com
DOI: https://doi.org/10.35633/inmateh-77-40

Keywords: *Precision seeding, Missing-seed detection and counting, Edge computing, YOLOv11n*

ABSTRACT

A lightweight vision-based model, GENet, is proposed to overcome the limitations of conventional missing-seed detection systems, which are highly sensitive to seed characteristics and constrained by slow response and complex configuration. Deployed on a small precision seeder featuring an oblique hook-shaped spoon-type metering device, GENet integrates Ghost Modules, C3Ghost structures, and an ECA attention mechanism. Experiments demonstrate an $mAP_{50–95}$ of 85.2%, accuracy of 99.9%, and 185 FPS inference speed on the Jetson AGX Xavier platform, while reducing model parameters by over 40%. Validation on the JPS-12 test bench confirms its robustness, providing an efficient solution for intelligent precision seeding.

摘要

为克服传统漏播检测系统易受种子特性影响、响应迟缓且结构复杂等问题，提出一种基于改进 YOLOv11n 架构的轻量化视觉模型 GENet。该模型部署于配备倾斜钩勺式排种装置的小型精量播种机上，集成了 Ghost 模块、C3Ghost 结构与 ECA 注意力机制。实验结果表明，在 Jetson AGX Xavier 平台上，GENet 的 $mAP_{50–95}$ 达到 85.2%，检测精度为 99.9%，推理速度达 185 FPS，参数量减少超过 40%。在 JPS-12 试验台上的验证结果表明，该模型具有良好的鲁棒性，为智能精量播种提供了一种高效的解决方案。

INTRODUCTION

Hilly and mountainous regions account for approximately 70% of China's total land area *(Luo, 2011)*, making the improvement of agricultural mechanization in these areas a critical priority. At present, there is a significant demand for precision seeding equipment suited to such terrains. Precision seeding technology not only enhances land utilization efficiency and seeding uniformity but also contributes to increased crop yields. However, missing seeds remain a notable challenge in precision sowing operations. Its occurrence is closely related to factors such as seed box depletion, metering device malfunction *(Che et al., 2017)*, complex field environments, and non-uniform travel speed of the seeder *(Zhang et al., 2022; Yang et al., 2022)*, all of which can ultimately lead to reduced crop productivity. Therefore, integrating a missing-seed detection and counting module into the seed metering device is of great importance. Such a module can (1) provide real-time alerts to operators in the event of abnormal seeding, thereby supporting timely inspection and reseeding, and (2) record the entire seeding process to quantitatively evaluate operational performance.

In recent years, scholars worldwide have developed a variety of sensor-based techniques for missing-seed detection and counting. *Wang et al. (2023)* designed a mechanical device that integrates missing-seed detection and reseeding functions. The device continuously monitors the filling state of the primary seed cells via a cross-type probe rod and actuates a locking lever to control the reseeding mechanism. However, this approach exerts mechanical pressure on the seeds, which may cause physical damage. *Okopnik and Falate (2014)* utilized infrared sensors and microcontrollers to monitor maize seed spacing, while *Zhang Xuejun et al. (2022)* employed a laser through-beam sensor to detect seed pickup conditions in cotton precision hill planters. These optical methods, however, offer limited detection ranges and require high installation precision, making them better suited for internal metering systems in compact planters. *Zhang et al. (2022)* proposed a fiber-optic sensor–based detection and automatic compensation method, whereas *Zagainov et al. (2023)* developed

a line-laser and phototransistor-array counting sensor capable of scanning the entire discharge region at the seed-tube outlet. Yet, the downstream placement of such sensors allows insufficient time for reseeding. *Wang et al. (2024)* introduced a spatial-capacitance-based detection method suitable for large seeds such as potatoes, though its sensitivity to small seeds remains limited due to minimal capacitance variation. *Ding et al. (2019)* designed a thin laser–photovoltaic monitoring device that achieved detection accuracies of 98.6% for rapeseed and 95.8% for wheat, although performance varied across seed types. *Rossi et al. (2023)* combined piezoelectric sensors with a VTPD-AM algorithm to monitor the seeding of maize, soybean, and sunflower, and *Ding et al. (2017)* enhanced this approach by introducing a recessed-substrate piezoelectric film structure that improved the resolution of high-frequency seed-flow detection. However, piezoelectric methods rely on contact-based sensing, which can disturb seed motion and impair metering accuracy. *Karayel et al. (2006)* employed high-speed imaging to analyze seed fall velocity and spacing for seeding-quality assessment, but the high cost and operational complexity of such equipment hinder large-scale field adoption. *Karimi et al. (2015)* developed an automated acoustic detection system that captures voltage-pulse signals produced when wheat, maize, and pelleted tomato seeds strike a steel plate; however, this method is highly susceptible to ambient noise and vibration. *Xie et al. (2022)* utilized a 24 GHz microwave-signal generation and intermediate-frequency pulse-analysis technique combined with a voltage-signal computational model for maize seed detection, though its accuracy deteriorates under high-humidity conditions.

The rapid development of deep learning has introduced new opportunities for agricultural operation monitoring *(Wen et al., 2025)*. Single-stage object detection algorithms, represented by the YOLO series, have been widely applied in smart agriculture tasks such as fruit and vegetable harvesting and pest monitoring *(Wen et al., 2024; Tao et al., 2024)*. However, their application in seeder missing-seed detection remains limited. *Zhao et al. (2025)* adopted an improved YOLOv5s-based detection and tracking algorithm to evaluate the performance of high-speed maize metering devices; yet, their work remained confined to laboratory settings without field validation.

To address these challenges, this study focuses on a small precision seeder equipped with an oblique hook-shaped spoon-type metering device, which is well-suited for hilly and mountainous terrains. A novel missing-seed detection and counting model, termed GENet, is developed based on an improved YOLOv11n architecture. The proposed approach accurately identifies missing seeds and performs real-time counting, providing sufficient response time for reseeding operations. Compared with traditional sensor-based methods, GENet is independent of seed type and less affected by seeding speed, provided that the camera frame rate is adequate. These advantages highlight its superior robustness and strong potential for practical application in intelligent precision seeding systems.

MATERIALS AND METHODS

Structure and Working Principle of the Seed Metering Device

The Oblique Hook-Shaped Spoon-Type Small Precision Seed Metering Device mainly comprises a seed box, spoon wheel, and side cover (Fig. 1). The seed box features a bottom discharge outlet, while the side cover is bolted to the housing. The spoon wheel rotates smoothly around a central shaft, and its outer edge contains V-shaped grooves with seed scoops, forming cavities that hold single seeds such as maize or soybean. During rotation, the device sequentially performs seed picking, cleaning, and dropping, achieving single-grain precision metering. Its compact and stable design ensures reliable operation for subsequent missing-seed detection.

Fig. 1 - Structure of the oblique hook-shaped spoon-type precision seed metering device

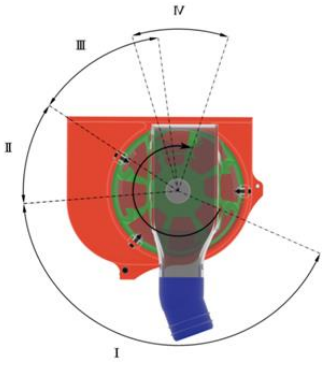

Fig. 2 - Working principle of the spoon-wheel seed metering device

As shown in Fig. 2, the metering process includes four stages: seed picking, primary cleaning, secondary cleaning, and seed dropping. In seed picking, seeds enter the spoon cavity by gravity and agitation. During cleaning, excess seeds fall off, leaving one per cavity. Secondary cleaning removes residual seeds while retaining a single seed for delivery. In the final stage, as the spoon wheel reaches the outlet, the V-shaped groove releases the seed, which falls by gravity through the guide tube into the furrow. The coordinated mechanism ensures stable, continuous, and precise single-seed delivery, forming a solid basis for real-time visual monitoring and precision seeding.

Image Acquisition and Dataset Construction

Image acquisition

To capture dynamic images of the oblique hook-shaped spoon at the seed outlet during operation, an image acquisition system was installed near the working area of the precision seed metering device. An Intel RealSense D435i camera was mounted on a dedicated base 5 cm from the spoon surface to ensure a stable imaging position and consistent viewing angle, thereby minimizing image deviations caused by vibration or displacement. This setup enabled continuous and clear recording of the entire seeding process without interfering with normal operation.

For missing-seed detection and seeding count, three categories of images were collected: (1) spoon carrying a seed, (2) spoon without a seed, and (3) spoon back. The primary classification criterion was whether the spoon carried a seed, enabling distinction between normal seeding and missing-seed states, while the total number of seeding events was determined by identifying spoon backs.

To ensure image clarity and lighting stability, LED lights were installed at the detection position for illumination. To enhance contrast between the target and background, the spoons were fabricated from white PLA, and other components were made of black PLA, thereby preventing color interference with the seeds. This configuration effectively differentiates missing-seed events from normal seeding states and provides reliable visual data for subsequent performance analysis. The image acquisition environment is shown in Fig.3.

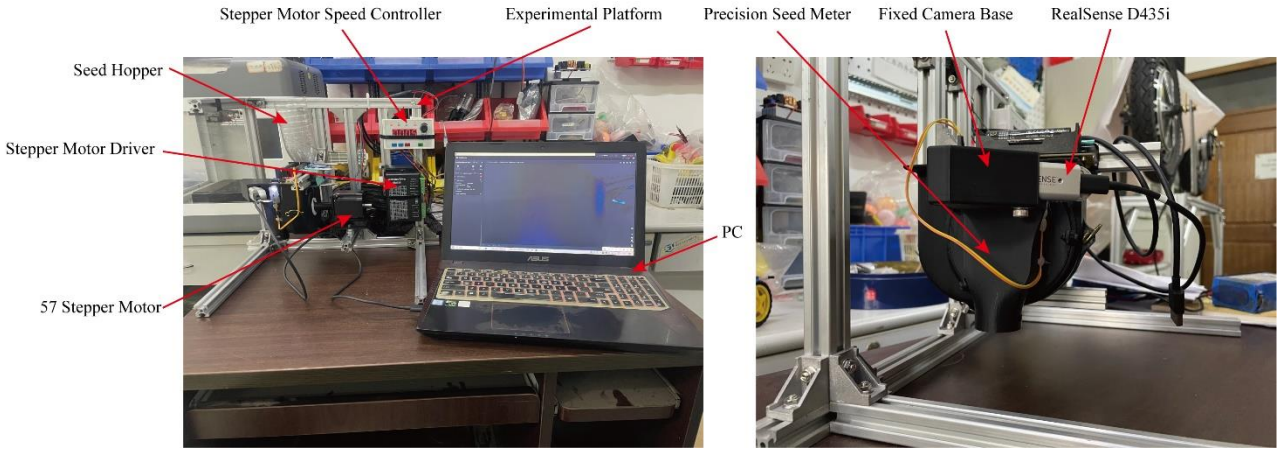

Fig. 3 - Image acquisition setup

During dataset construction, the camera recorded videos of the seeding window under real operating conditions, saved in MP4 format. Video frames were extracted to form the raw dataset. Using the LabelImg tool, image targets were annotated as vacant (empty spoon) or via (spoon back). The annotated dataset was divided into training, validation, and testing sets at a 7 : 2 : 1 ratio, comprising 2,100, 600, and 300 images, respectively.

ROI-Based Preprocessing and Data Augmentation

To reduce computational overhead and enhance inference efficiency on edge devices, a static Region of Interest (ROI) cropping strategy was employed during both dataset preprocessing and inference stages. This method retains only the task-relevant regions of the image while eliminating redundant background, thereby significantly reducing input data volume and accelerating model training and inference.

During dataset construction, ROI coordinates were determined using the LabelImg annotation tool and applied via a Python script to crop the original images, generating samples containing only the detection region. As shown in Fig. 4(a–c), the yellow dashed box represents the defined ROI, while the excluded background region—approximately 95% of the total image—is unrelated to the detection task. After ROI cropping, the image file size decreased from 984 KB to 108 KB, as illustrated in Fig. 4(d–f). During inference, the same ROI

parameters were applied to incoming frames before model processing, and the detection results were subsequently mapped back to the original image for visualization and traceability. This strategy effectively reduces storage and computation requirements while maintaining detection accuracy, achieving a significant acceleration in both training and inference processes.

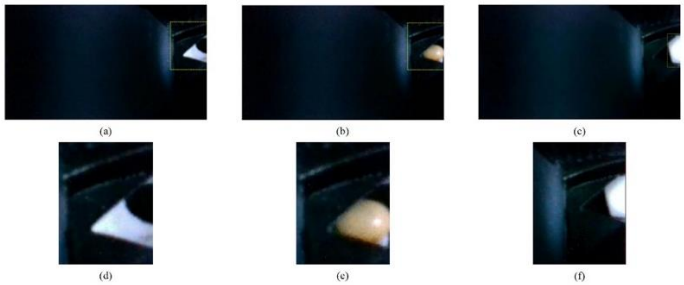

Fig. 4 - Dataset images before and after ROI preprocessing

In practical field applications, the oblique hook-type precision seed metering device is typically mounted on small power platforms (e.g., walking tractors) operating at high rotational speeds over uneven terrain. These complex conditions often induce camera vibration or transient sensor faults, resulting in blurred or distorted images. To realistically simulate such conditions, three types of synthetic disturbances were introduced into the ROI-cropped images: (1) salt-and-pepper noise, mimicking pixel-level sensor faults; (2) Gaussian blur, representing motion blur caused by vibration; and (3) combined noise and blur, reflecting compound interference commonly observed in field operations. As shown in Fig. 5, the processed images effectively reproduce the visual degradation typical of field seeding environments. This enhanced dataset provides a reliable foundation for evaluating and optimizing the robustness of the proposed detection model.

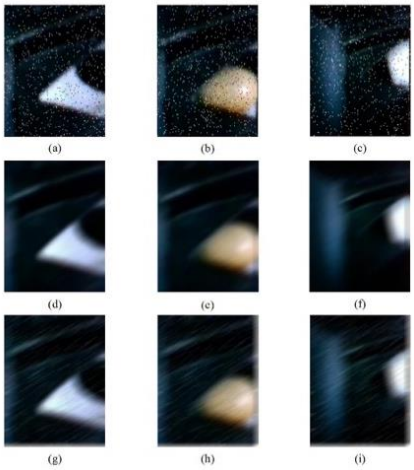

Fig. 5 - ROI-cropped images with simulated disturbances

Detection model based on improved YOLOv11

Ghost Lightweight Network

Since the seed metering device must be mounted on a small power platform for field operation, its overall structure needs to remain compact and lightweight, while still accommodating a camera for real-time image acquisition. Consequently, the missing-seed detection model must be deployable on edge computing devices with limited computational resources, requiring a balance between detection accuracy and computational efficiency. To achieve this, the Ghost Module was introduced as a core component to enable high-performance feature extraction under low computational cost.

The Ghost Module generates additional ghost feature maps by applying a series of linear transformations to intrinsic feature maps from each convolutional channel, as shown in Fig. 6. These additional features enrich the model's representational capacity while significantly reducing computation compared with standard convolutional operations. Unlike conventional methods that rely on pointwise and depthwise convolutions to process spatial information, the Ghost Module first uses standard convolution to generate a subset of intrinsic feature maps, followed by low-cost linear transformations to expand the channel dimension and enhance feature diversity. Through identity mapping, it also preserves the semantic consistency between intrinsic and ghost features, minimizing information loss.

Building on this, the Ghost Bottleneck structure deepens the network by stacking two Ghost Modules to enhance feature extraction and representation capability, as illustrated in Fig.7. The first Ghost Module expands the channel dimension to increase feature diversity, while the second compresses it to match the original input dimension, thus controlling model complexity. A residual connection is incorporated to improve gradient flow, enhancing both training stability and efficiency.

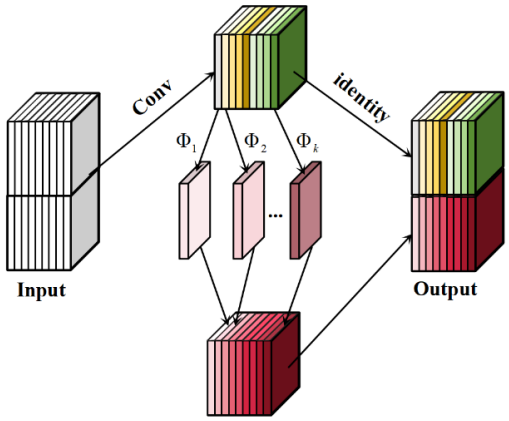

Fig. 6 - Structures of the Ghost Module

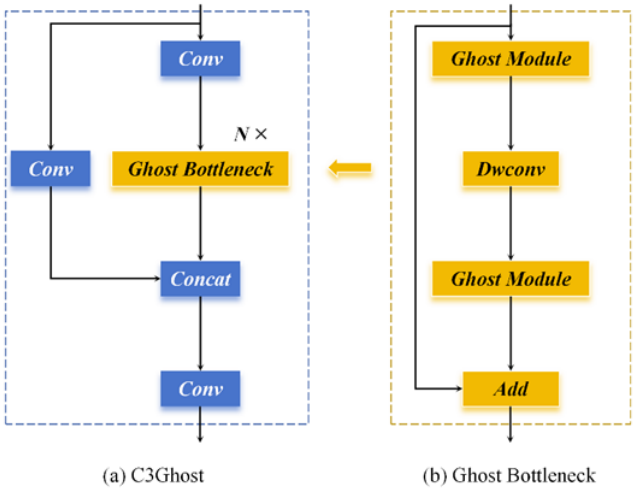

Fig. 7 - Structures of the Ghost Bottleneck and C3Ghost

Further, the C3Ghost module extends this design by stacking multiple Ghost Bottlenecks and introducing an additional shortcut branch composed of a single convolutional layer. This branch directly retains raw input information, preventing feature degradation in deeper layers, while providing a direct gradient propagation path to improve training convergence. The shortcut and main branches complement each other: the former preserves low-level details, and the latter extracts high-level abstract features. Overall, the C3Ghost module achieves an effective balance between lightweight computation and feature richness, making it highly suitable for edge-deployed missing-seed detection tasks.

Efficient Channel Attention (ECA) Mechanism

To enhance the model's ability to focus on key information while suppressing redundant or irrelevant features, the Efficient Channel Attention (ECA) mechanism was integrated into the proposed network. Compared with the traditional Squeeze-and-Excitation (SE) module, ECA avoids dimensionality reduction, thereby preserving inter-channel dependencies that might otherwise be weakened during compression.

The core idea of ECA is to employ a one-dimensional convolution to efficiently model local cross-channel interactions while maintaining dimensional consistency and low computational cost. As shown in Fig. 8, the ECA module first performs global average pooling on the input feature map to obtain global semantic information. A 1D convolution with kernel size k is then applied to capture local inter-channel dependencies. The resulting response is passed through a Sigmoid activation function to generate the channel-wise attention weights ω, which are computed as:

$$\omega = Sigmoid(1D_k(C)) \tag{}$$

where $1D_k$ denotes the one-dimensional convolution with kernel size k, and C represents the channel descriptor obtained through global average pooling. Finally, these weights are multiplied element-wise with the corresponding feature channels to enhance informative features and suppress irrelevant ones.

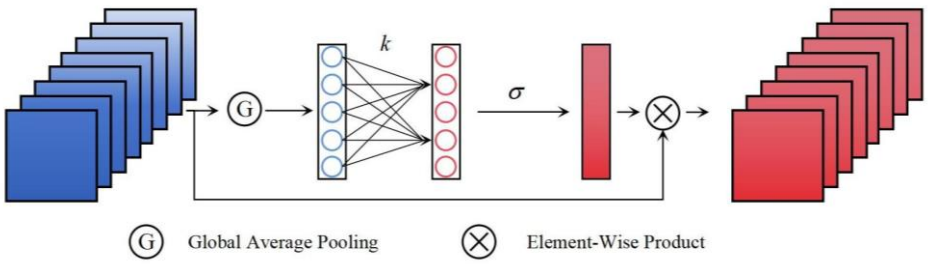

Fig. 8 - Structure of the ECA mechanism

This mechanism effectively improves feature representation while maintaining low computational complexity, resulting in a more robust and efficient detection performance under complex operational conditions.

GENet Model

To further improve the accuracy and stability of missing-seed detection, a lightweight detection model named GENet was developed based on the improved YOLOv11n architecture. GENet achieves a balanced trade-off between model compactness and detection performance. Its overall structure is illustrated in Fig. 9, and the main improvements are summarized as follows:

1. The standard convolutional layers in both the Backbone and Neck were replaced with Ghost Modules, which generate additional feature channels through low-cost linear transformations. This approach significantly reduces redundant convolutional operations while maintaining feature representation capability, thereby decreasing model parameters and computation cost and improving inference efficiency on edge devices.
2. The original C3k2 modules in the Backbone and Neck were replaced with C3Ghost modules, which incorporate Ghost Bottlenecks into the residual structure. The shortcut branch preserves input information and enhances gradient flow, while the main branch extracts deeper semantic features. Their complementary interaction improves feature representation. Compared with C3k2, C3Ghost achieves a better balance between lightweight design and detection accuracy, while substantially increasing inference speed.
3. The ECA mechanism was embedded at the high-level feature layer (P5) to efficiently capture local inter-channel dependencies via one-dimensional convolution. By adaptively assigning channel weights, ECA enhances the model's focus on key features and suppresses redundant information, thereby improving recognition ability and detection precision, particularly under complex background conditions.

Overall, GENet combines lightweight structural optimization with adaptive attention enhancement, achieving high detection accuracy, robustness, and real-time performance suitable for edge-deployed missing-seed detection tasks.

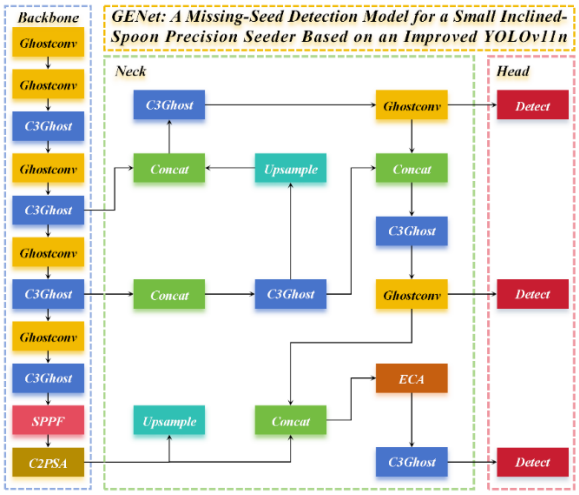

Fig. 9 - Overall architecture of the proposed GENet model

Experiments and Results

Experimental Environment and Parameter Settings

The experiments were conducted on a workstation running Windows 10 with an NVIDIA Quadro RTX 4000 GPU equipped with 8 GB of VRAM. The model was developed and trained using the PyTorch 1.31.1 deep learning framework with Python 3.10 as the programming language, and CUDA 12.1.0 for GPU acceleration. The detailed training parameter configurations are listed in Table 1.

Table 1

Training parameter settings

Training Parameter	Value	Training Parameter	Value
Optimizer	SGD	Epochs	100
Workers	0	Batch Size	16
Weight decay	0.0005	Warmup momentum	0.8

Comparison of Attention Insertion Positions

To determine the optimal insertion position of the Efficient Channel Attention (ECA) mechanism, comparative experiments were conducted within the Neck of the Ghost lightweight network. Specifically, the ECA module was inserted at different feature levels - P3, P4, and P5 - as well as in combined configurations involving two or three simultaneous insertions. The computational complexity and detection performance of each configuration were evaluated, as summarized in Table 2.

Table 2

Performance comparison of different ECA insertion positions

Position	Parameter (M)	Model size (MB)	GFLOPs (G)	Speed (FPS)	Precision (%)	mAP_{50-95} (%)
No	1.44	3.07	3.8	246.18	99.6	82.8
P3	2.04	4.23	7.5	240.58	99.3	84.6
P4	1.57	3.31	4.0	238.67	98.9	82.7
P5	1.52	3.23	3.9	242.90	99.9	85.2
P3+P4	1.83	3.82	7.3	234.71	99.9	84.7
P3+P5	2.04	4.23	7.5	236.81	99.9	84.2
P4+P5	1.57	3.31	4.0	225.59	99.9	83.6
P3+P4+P5	1.83	3.82	7.3	227.46	99.9	83.5

The results indicate that inserting the ECA mechanism at the P5 layer yields the best performance. Compared with the baseline YOLOv11n model, the GFLOPs increased by only 2.6%, while mAP_{50-95} improved by 2.4%, outperforming all other single-layer configurations. When the attention mechanism was inserted at multiple layers simultaneously, model complexity and computation increased substantially, but detection accuracy did not exceed that of the P5-only configuration (85.2%), and inference speed decreased accordingly.

This trend is closely related to the semantic characteristics of feature maps. The P5 layer features lower spatial resolution but richer semantic information, making it more suitable for channel attention enhancement. In the present study, the ROI-cropped images have relatively low resolution, with large and semantically rich target regions containing limited fine details. Therefore, integrating the ECA mechanism at the P5 layer of the Neck effectively improves detection accuracy with minimal computational overhead, achieving an optimal balance between lightweight design and high precision.

Ablation Study

To validate the effectiveness of the Ghost Module and the ECA mechanism, ablation experiments were conducted using YOLOv11n as the baseline model under identical experimental conditions and the same test dataset. The results are summarized in Table 3.

Table 3

Ablation study of Ghost and ECA mechanisms

Ghost	ECA-P5	Parameters (M)	Model size (MB)	GFLOPs (G)	Precision (%)	mAP_{50-95} (%)
×	×	2.58	5.21	6.3	99.2	83.1
√	×	1.44	3.07	3.8	99.6	82.8
×	√	2.67	5.36	6.4	99.7	85.0
√	√	1.52	3.23	3.9	99.9	85.2

The results demonstrate that incorporating the Ghost lightweight network into YOLOv11n reduces the number of parameters by 44.2% and GFLOPs by 39.7%, while precision and mAP_{50-95} increase by 0.4% and 1.7%, respectively. This indicates that the Ghost Module effectively enhances feature representation while significantly reducing redundant computation.

Furthermore, introducing the ECA attention mechanism at the P5 layer of the Neck improves precision and mAP_{50-95} to 99.7% and 85.0%, respectively. This improvement results from ECA's ability to model cross-channel dependencies and adaptively assign feature weights, thereby emphasizing key features. However, this enhancement also leads to moderate increases in model parameters and computation.

Finally, combining both the Ghost Module and ECA mechanism forms the proposed GENet model. GENet achieves a 41.1% reduction in parameters, 38.0% smaller model size, and 41.1% reduction in GFLOPs, while attaining a precision of 99.9% and mAP_{50-95} of 85.2%.

These results confirm the complementary synergy between lightweight structural optimization and attention-based feature enhancement, enabling GENet to achieve an optimal balance between model compactness and detection performance.

Comparative Experiments

To further validate the superiority of the proposed GENet model over other lightweight object detection networks, comparative experiments were conducted using YOLOv7-tiny, YOLOv8n, YOLOv10n, and the baseline YOLOv11n under identical experimental conditions and the same test dataset. The results are summarized in Table 4.

Table 4

Comparison of GENet with other lightweight detection models

Model	Parameters (M)	Model Size (MB)	GFLOPS (G)	Speed (FPS)	Precision (%)	mAP_{50-95} (%)
YOLOv7-tiny	7.1	12.3	13.2	216.18	98.1	82.1
YOLOv8n	3.2	6.3	8.7	231.52	98.5	82.7
YOLOv10n	2.7	5.8	6.7	236.18	99.0	82.8
YOLOv11n	2.58	5.21	6.3	236.69	99.2	83.1
GENet	1.52	3.23	3.9	242.90	99.9	85.2

The results indicate that GENet outperforms all comparative models in both detection accuracy and lightweight efficiency. GENet achieves an mAP_{50-95} of 85.2%, exceeding YOLOv7-tiny, YOLOv8n, YOLOv10n, and YOLOv11n by 3.1%, 2.5%, 2.4%, and 2.1%, respectively. In terms of model complexity, GENet contains only 1.52 M parameters, with 3.9 GFLOPs, a model size of 3.23 MB, and an inference speed of 242.9 FPS, all superior to the comparison models. These results confirm that GENet maintains high accuracy with minimal computational cost, demonstrating a clear advantage in performance–efficiency trade-off design.

To further verify practical detection performance, the test images were evaluated using both GENet and YOLOv11n, as shown in Fig. 10, where red ellipses highlight missed detections. In both spoon-back and vacant-cavity detection scenarios, YOLOv11n exhibited five missed detections, while GENet showed only one, indicating significantly higher accuracy and stability under complex conditions.

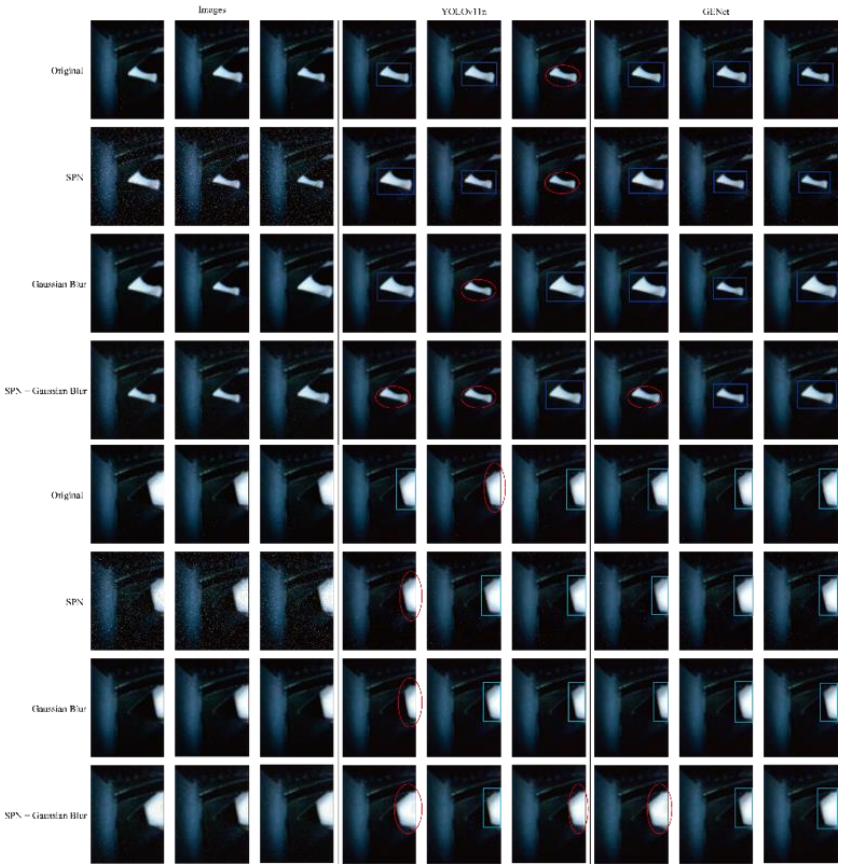

Fig. 10 - Visual comparison of detection performance between YOLOv11n and GENet

The missed detections of YOLOv11n were mainly caused by strong reflections on the spoon back, partial occlusions, motion blur due to high-speed rotation, and weakened cavity textures disturbed by salt-and-pepper noise (SPN). In contrast, GENet benefits from the synergistic effect of lightweight design and enhanced discrimination capability:

- The Ghost Module improves inference speed and reduces latency, narrowing the window for motion-induced missed detections.
- The C3Ghost module strengthens the extraction of geometric and curvature features, maintaining stability under partial occlusion or pose variation.
- The ECA attention mechanism at the P5 layer adaptively reweights key channels, effectively suppressing interference from reflection, SPN noise, and motion blur.

Overall, GENet demonstrates superior robustness and precision across both detection tasks. Its lightweight architecture not only ensures efficient deployment on edge computing devices, but also provides a reliable and high-performance solution for missing-seed detection and counting in precision seeders.

Edge Deployment and Experiment

To evaluate the deployment performance of the improved GENet model on edge computing devices, the NVIDIA Jetson AGX Xavier platform was selected. To further enhance inference speed, the model was accelerated using the TensorRT inference engine. On this platform, GENet achieved an inference speed of 185 FPS, representing a 4.02× improvement compared with the pre-acceleration speed of 41 FPS. These results demonstrate that the optimized network not only possesses strong lightweight characteristics but also maintains high inference efficiency under hardware acceleration.

During the actual operation of the oblique hook-type precision seed metering device, the Intel RealSense D435i camera operated at 60 FPS. In comparison, the 185 FPS inference speed of GENet on the Jetson AGX Xavier fully meets the real-time processing requirements of such video streams, laying a solid foundation for its embedded application in precision seeding equipment.

Furthermore, to verify the applicability and generalization of the proposed GENet model in real-world seeding scenarios, on-site experiments were conducted. During the tests, real-time video streams were captured using the Intel RealSense D435i camera and processed online by the GENet model. The results are shown in Fig. 11.

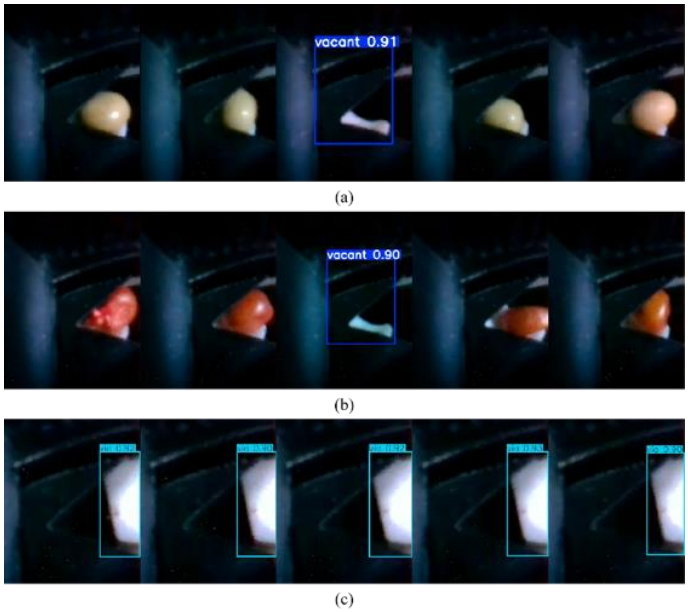

Fig. 11 - Real-time missing-seed detection and counting results of the GENet model during maize and soybean seeding

As shown in Fig. 11, GENet exhibited excellent robustness in both maize and soybean seeding processes, achieving stable missing-seed detection and counting performance. Across continuous video frames, no significant missed or false detections were observed, confirming the model's strong reliability and real-time capability. These findings provide a promising technical foundation and research pathway for intelligent monitoring of precision seeding operations.

Verification on the Precision Seeder Test Bench

To verify the reliability of the GENet model for missing-seed detection and counting under actual operating conditions of the oblique hook-type precision seed metering device, on-site experiments were conducted using the JPS-12 seeder performance test bench, as shown in Fig. 12. During the tests, an Intel RealSense D435i depth camera was used to capture seeding images in real time, while the GENet model was deployed on the NVIDIA Jetson AGX Xavier platform for edge-based real-time detection and computation.

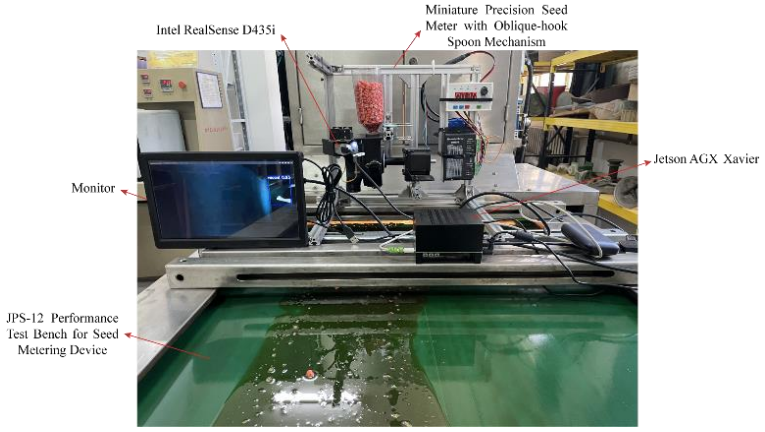

Fig. 12 - Experimental setup

Experiments were performed under spoon-wheel rotational speeds of 10 rpm, 20 rpm, and 30 rpm for both maize and soybean, with 10 repetitions per condition and 100 seeds per trial. The GENet model was responsible for real-time missing-seed detection and counting. To visualize performance, the results were plotted, as illustrated in Fig.13. The missing-seed detection results show that, as the spoon-wheel speed increased, the actual missing-seed rate of both crops rose accordingly, reflecting the objective trend of reduced metering stability at higher speeds. Meanwhile, the detection results of GENet closely matched the actual measurements: in maize experiments, the maximum deviation between detected and actual missing-seed rates was less than 0.3%, and in soybean tests, it was below 0.4%. For both crops, GENet accurately captured the trend of increasing missing-seed rate and maintained high detection accuracy even under high-speed (30 rpm) conditions. The counting results, shown in Fig.14, indicate that GENet achieved extremely high counting accuracy across all speeds. The average counting accuracy reached 99.86% for maize and 99.90% for soybean. Although a slight decline was observed with increasing rotational speed, the overall performance remained stable and consistently above 99.5%. These results confirm the high reliability of GENet in counting tasks and its ability to meet the stringent accuracy requirements of precision seeding.

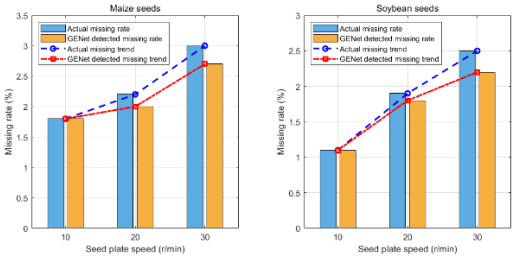

Fig. 13 - GENet performance in missing-seed detection

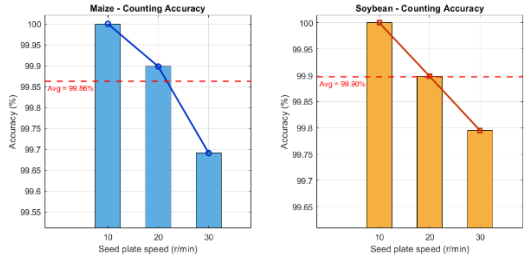

Fig. 14 - GENet performance in counting

In summary, GENet demonstrated stable and high-precision performance across different crops and operating speeds, with no evident missed or false detections. The results highlight the model's robustness and generalization capability, confirming the feasibility of deep learning–based vision systems for real-time missing-seed monitoring and counting in precision seeding applications. This provides a solid technical foundation for the practical deployment of intelligent visual monitoring in field seeding operations.

CONCLUSIONS

This study developed a lightweight vision-based missing-seed detection and counting model, GENet, which integrates Ghost Modules, C3Ghost structures, and an ECA attention mechanism to achieve an effective balance between accuracy and computational efficiency. The results confirm that deep learning models can be feasibly deployed on edge devices, offering a sensor-free and adaptive solution for precision seeding.

Compared with existing lightweight networks such as YOLOv7-tiny, YOLOv8n, YOLOv10n, and YOLOv11n, GENet achieved superior accuracy (99.9%) and inference speed (185 FPS) with fewer parameters. This demonstrates that structural optimization and attention enhancement not only reduce computational cost but also strengthen robustness under variable field conditions—an essential factor for real-time agricultural applications.

Bench validation on the JPS-12 precision seeder test platform further verified the model's stability and generalization, with deviations between detected and actual missing-seed rates remaining below 0.4%. These findings highlight GENet's capability for multi-crop adaptation and practical deployment in intelligent precision seeding systems, providing valuable insights for integrating edge computing and deep learning in future smart agricultural machinery.

ACKNOWLEDGEMENT

This research was supported by the Shaanxi Provincial Key R&D Program (Grant No. 2023-ZDLNY-62): Development and Industrialization of Unmanned Operational Equipment for Soybean–Maize Strip Intercropping.

REFERENCES

[1] Che, Y., Wei, L. G., Liu, X. T., et al. (2017). Design and experiment of infrared monitoring system for sowing quality of no-tillage seeder. *Transactions of the Chinese Society of Agricultural Engineering*, 33.

[2] Ding, Y. C., Yang, J. Q., Zhu, K., et al. (2017). Design and experiment of seed-flow sensing device for rapeseed precision metering. *Transactions of the Chinese Society of Agricultural Engineering*, 33(9).

[3] Ding, Y. C., Zhu, K., Wang, K. Y., et al. (2019). Development of a thin-laser and silicon solar-cell-based monitoring device for small-seed flow. *Transactions of the Chinese Society of Agricultural Engineering*, 35(8).

[4] Jiayv, S., Qingzhong, K., & Yanghao, L. (2024). Pod-pepper target detection based on improved YOLOv8. *INMATEH – Agricultural Engineering*, 74(3).

[5] Karayel, D., Wiesehoff, M., Özmerzi, A., et al. (2006). Laboratory measurement of seed-drill seed spacing and velocity of fall of seeds using a high-speed camera system. *Computers and Electronics in Agriculture*, 50(2), 89–96.

[6] Karimi, H., Navid, H., & Mahmoudi, A. (2015). Online laboratory evaluation of seeding-machine application by an acoustic technique. *Spanish Journal of Agricultural Research*, 13(1), 202.

[7] Luo, X. W. (2011). Reflections on the development of agricultural mechanization in hilly and mountainous areas. *Agricultural Machinery Science and Technology Extension*, (2), 17–20.

[8] Okopnik, D. L., & Falate, R. (2014). Usage of the DFRobot RB-DFR-49 infrared sensor to detect maize seed passage on a conveyor belt. *Computers and Electronics in Agriculture*, 102, 106–111.

[9] Rossi, S., Scola, I. R., Bourges, G., et al. (2023). Improving the seed detection accuracy of piezoelectric impact sensors for precision seeders. Part I: A comparative study of signal-processing algorithms. *Computers and Electronics in Agriculture*, 215, 108449.

[10] Tao, S., Wen, S., Hu, G., et al. (2024). Improved YOLOv8n-based detection of grapes in orchards. *INMATEH – Agricultural Engineering*, 74(3), pp.473-484. DOI: https://doi.org/10.35633/inmateh-74-42

[11] Wang, G., Yang, X., Sun, W., et al. (2024). Potato seed-metering monitoring and improved miss-seeding catching-up compensation control system using spatial-capacitance sensor. *International Journal of Agricultural and Biological Engineering*, 17(4), 255–264.

[12] Wang, Z., Ming, J., Wang, Q., et al. (2023). Design and experiment of a mechanical device for missing-seed detection and reseeding. *Journal of Chinese Agricultural Mechanization*, 44(10), 21.

[13] Wen, S., Ge, Y., Wang, Y., et al. (2025). Efficient and comprehensive visual solution for a smart apple-harvesting robot in complex settings via multi-class instance segmentation. *International Journal of Agricultural and Biological Engineering*, 18(4), 200–215.

[14] Wen, S., Zhou, J., Hu, G., et al. (2024). PcMNet: An efficient lightweight apple-detection algorithm in natural orchards. *Smart Agricultural Technology*, 9, 100623.

[15] Xie, C., Yang, L., Zhang, D., et al. (2022). Design of smart seed sensor based on microwave-detection method and signal-calculation model. *Computers and Electronics in Agriculture*, 199, 107178.

[16] Yang, S., Zhai, C., Gao, Y., et al. (2022). Planting-uniformity performance of motor-driven maize precision seeding systems. *International Journal of Agricultural and Biological Engineering*, 15(5), 101–108.

[17] Zagainov, N., Kostyuchenkov, N., Huang, Y. X., et al. (2023). Line-laser-based sensor for real-time seed counting and seed-miss detection for precision planters. *Optics & Laser Technology*, 167, 109742.
[18] Zhang, C., Xie, X., Zheng, Z., et al. (2022). A plant unit related to missing-seeding detection and reseeding for maize precision seeding. *Agriculture*, 12(10), 1634.
[19] Zhang, X. J., Zhang, H. T., Shi, Z. L., et al. (2022). Design and experiment of cotton precision hill-drop seeder seed-taking monitoring system. *Transactions of the Chinese Society of Agricultural Engineering*, 38(5).
[20] Zhao, P., Wu, X., Cheng, H., et al. (2025). Performance evaluation of a high-speed maize seed-metering device using an improved YOLOv5s object-detection and tracking algorithm. *Smart Agricultural Technology*, 100997.